


## Research Article

# Mine Ground Pressure Monitoring and Early Warning Based on Deep Learning Data Analysis

Yigai Xiao <sup>1,2</sup>, Hongwei Deng,<sup>1</sup> Zhimou Xie,<sup>2,3</sup> and Hongbin Lu<sup>4</sup>

<sup>1</sup>*School of Resources and Safety Engineering, Central South University, Changsha, 410083 Hunan, China*

<sup>2</sup>*Sinosteel Maanshan General Institute of Mining Research Co., Ltd., Maanshan, 243000 Anhui, China*

<sup>3</sup>*Sinosteel Nanjing Huaxin Technology Co. Ltd., Nanjing, 211100 Jiangsu, China*

<sup>4</sup>*Wangjiang University of Technology, Maanshan, 243000 Anhui, China*

Correspondence should be addressed to Yigai Xiao; [xiaoyi421@csu.edu.cn](mailto:xiaoyi421@csu.edu.cn)

Received 11 February 2022; Revised 22 March 2022; Accepted 13 April 2022; Published 27 April 2022

Academic Editor: Chia-Huei Wu

Copyright © 2022 Yigai Xiao et al. This is an open access article distributed under the Creative Commons Attribution License, which permits unrestricted use, distribution, and reproduction in any medium, provided the original work is properly cited.

In order to ensure the safe mining of kilometer mining working surface threatened by impact ground pressure, a metal mine ground pressure monitoring and early warning based on deep learning data analysis are proposed. This paper expounds the theoretical basis of rock burst, analyzes the inducing factors of deep well rock burst, analyzes and introduces the classification of rock burst, focuses on the progressive failure process of rock burst and standard of rock fracture depth of deep ore and rock in a metal mine, carries out triaxial stress-strain test on the core in the laboratory, and evaluates the tendency of rock burst for deep ore and rock through elastic strain generation, strength brittleness coefficient method, and deformation brittleness coefficient method. The real-time monitoring and early warning system of rock burst can monitor the dynamic change of advance stress in the working face in real time and give real-time early warning to the dangerous area and degree of rock burst. The experimental results show that the working face enters the fault affected area when it advances 170 m in front of the fault. When the working face advances to 100 m in front of the fault, it enters the high stress area formed by the superposition of fault tectonic stress and mining stress. When the working face advances to 40 m in front of the fault, the stress reaches the maximum. Therefore, the system can accurately predict the impact risk area and its risk degree and realize the safe mining of high impact risk face.

## 1. Introduction

Nonferrous metal mines are poor, rich mines; small mines, large, large mines, serious mineral resources gap, metal mining technology directly affects China's national defense security and the construction of an all-round well-off society. At the present stage, some mining equipment in China has realized large-scale automation, intelligent mining technology has been continuous or semicontinuous, and mining production and management have been widely used in computer technology, which has effectively promoted the development of metal mining industry. In recent years, with the increase of mining depth, mining conditions have become more and more difficult. Dynamic disasters such as rock burst and metal mine earthquake have become the main threat to safety production in mining areas. In the field

of rock burst monitoring and prediction, electromagnetic radiation monitoring method and drilling cuttings method are widely used [1]. However, due to the complexity of underground and electromagnetic environment in some mines, it has a great impact on the monitoring results of electromagnetic radiation monitoring method, resulting in large errors in the monitoring results. The amount of drilling cuttings is a comprehensive index including mining stress, mineral property, and outburst environment, which is more practical and reliable, but its prominent disadvantages are the danger of operators in the implementation process, individual operation errors, and continuous monitoring, resulting in the omission of useful information [2]. In this regard, many experts and scholars have also conducted many professional and in-depth studies on rock burst disaster in theory and numerical simulation analysis, but the

research on microseismic ground pressure online monitoring technology has made little progress due to its late start and lack of core technology [3].

The mining industry was mainly developed in the 1950s and 1960s; due to the limited technology level at that time, most nonferrous metal mines greatly reduced or even exhausted resources after decades of mining. Most of the existing nonferrous metal mines have entered the middle and late mines. The import volume of nonferrous metal minerals is increasing year by year, while industrialization is still in a state of rapid development. In the development of modern economy, along with the further development of industrialization, the economic consumption of nonferrous metals will still increase greatly, and the local mineral resources are not enough to maintain the economic development. Deep mining is the inevitable trend of the mining industry, and rock explosion disaster is the inevitable phenomenon of high stress and deep mining ground pressure. Studying the law of deep well ground pressure activity is the basis for the control of rock explosion such as ground pressure disaster. Deep mining is the inevitable trend of mining industry. Rock burst disaster is the inevitable phenomenon of ground pressure in high stress deep mining. Studying the law of deep well ground pressure activity is the basis of controlling rock burst and other ground pressure activities. In this paper, the rock burst tendency is evaluated from the rock burst inducing factors, progressive failure process, and mechanical parameters obtained from rock mechanics experiments. Combined with the most advanced microseismic monitoring technology, the rock burst is deeply studied, and the application of microseismic monitoring technology in deep well mines is emphatically analyzed. The law of ground pressure activity in deep wells is analyzed and studied based on microseismic data. Finally, a three-level early warning model is established [4, 5]. This has a certain role in promoting the application of microseismic monitoring technology in underground mines. The three-level early warning model of deep well rock burst based on microseismic has certain reference and practical value for other deep well mines with similar ground pressure disasters [6]. The ground pressure monitoring technology and equipment are shown in Figure 1.

## 2. Literature Review

Robinson et al. used microseismic phenomenon to study the rock burst problem in the mining process of deep well stope and used seismological theory to accurately locate the location of rock burst, which promoted the use of microseismic phenomenon to control and study the ground pressure phenomenon, especially the rock burst problem [7]. Through investigation and analysis, Worthington and Foley found that there are mainly the following problems in the monitoring and prevention of rock burst: there are a large number of rock burst mines; rock burst mines are widely distributed regionally, with great differences in geological and mining technical conditions. The factors affecting the occurrence of rock burst are different, and the occurrence mechanism, monitoring, and early warning mechanism of rock burst

are different [8]. Kanabkaew et al. conducted in-depth research on the characteristic changes of microseismic signals before and after rock burst disaster in hard rock and found that before rock burst, the microseismic signal strength will continue to increase; that is, microseismic signals with strong intensity will appear, and then there will be a trend of sudden energy drop, followed by rock burst or other ground pressure disasters [9].

Río et al. put forward that there are many rock burst monitoring parameters and equipment manufacturers, which makes it difficult to establish a unified and standardized data interface between monitoring systems and similar systems produced by different manufacturers. There is a lack of "time-space" correlation between rock burst monitoring parameters, and most of them are single index early warning, and the early warning results cannot realize real-time joint analysis. The accuracy of monitoring and early warning results needs to be further improved [10]. Romashchenko et al. used statistical theory to study microseismic activity and ore recovery rate, evaluated the risk degree of metal mine earthquake according to the energy release value in a certain period of time and space, and successfully applied it in local coal metal mines [11]. Chen conducted in-depth research on microseismic signal identification and microseismic precursor law of ground pressure disaster and achieved good confirmation in the successful early warning of ground pressure disaster [12]. Ma et al. systematically studied the phenomenon of deep well rock burst by the South African microseismic system established by Huize Lead zinc metal mine and obtained systematic conclusions [13]. Oz et al. developed a new explosion-proof microseismic monitoring system suitable for coal metal mine environment, conducted a lot of research on the prediction and prevention of coal mine ground pressure disaster, and achieved good results [14]. Sengupta et al. introduced the South African microseismic monitoring system, conducted in-depth research on the law of rock mass damage activity and microseismic activity caused by mining disturbance, and achieved good results [15].

Based on this research, this paper proposes a mine ground pressure monitoring and early warning system based on in-depth learning data analysis, develops a set of real-time monitoring and early warning system of rock burst which can realize continuous, reliable, safe monitoring and early warning of rock burst risk area and risk degree and successfully apply it to many mines threatened by rock burst, and achieves good results.

## 3. Research Methods

### 3.1. Basic Principle of Real-Time Online Monitoring and Early Warning System of Rock Burst Based on Deep Learning

**3.1.1. Convolutional Neural Network.** As one of the important methods of deep learning, convolutional neural networks use the cognitive connection, feature abstraction, and autonomous learning ability of convolutional neural networks to simulate the monitoring and early warning process online when undergoing shock compaction in deep

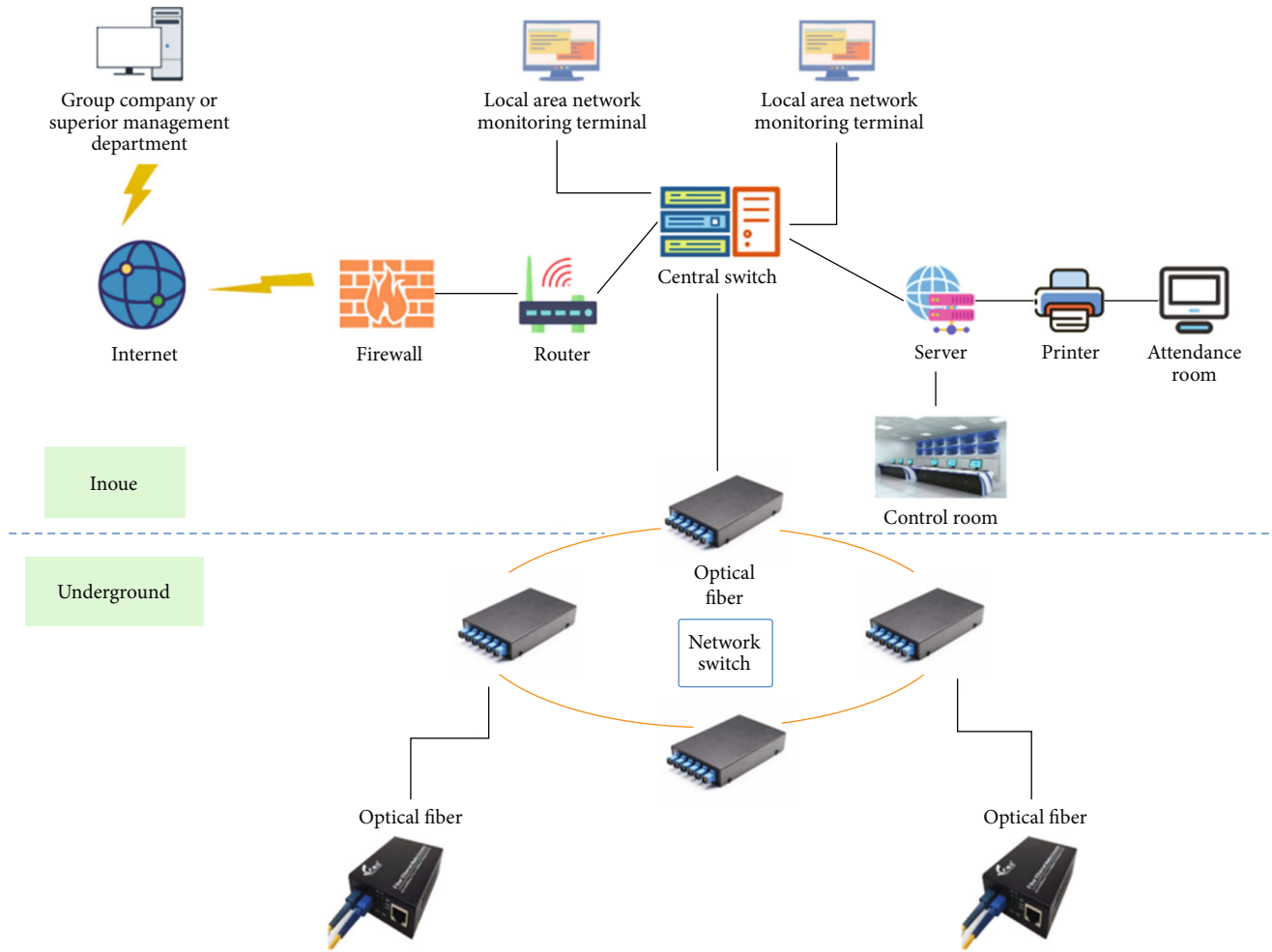


FIGURE 1: Ground pressure monitoring technology and equipment.

learning [16]. Convolution neural network (CNN) was originally proposed based on the naturally formed human visual system, with natural advantages in image recognition and feature extraction [17, 18]. The biggest feature of the deep learning convolutional network is the nonlinear correspondence between the output feature graph and the input graph, so the convolutional neural network can be regarded as a complex filter. CNN mainly learns the features of images in different aspects through convolution, pooling, and full-link operations, which is in line with the process of cognitive images through the human visual field. When observing and learning an image, human beings first pay attention to its brightness, contrast, color, and other macro information, followed by local information such as edges and corners and lines, and then the extraction of more complex information such as geometry and patterns, and finally form the cognition of the image in the human brain [19].

*3.1.2. Early Warning Principle and Setting of Early Warning Value of Real-Time Monitoring and Early Warning System of Rock Burst.* The process of real-time online monitoring and early warning of rock burst is simulated by using the cognitive connection, feature abstraction, and autonomous learning ability of deep learning. The real-time monitoring and

early warning system of rock burst predicts rock burst based on the equivalent drilling cuttings method; that is, in the area with rock burst risk, before rock burst occurs, the mining stress increases gradually, and the rock burst may occur only when the stress reaches the rock failure limit, and at this time, the amount of drilling cuttings will exceed the rated safety index. Therefore, the relationship between the change law of stress increment and the amount of drilling cuttings can be determined by analyzing the monitoring data, and the amount of drilling cuttings can be obtained indirectly according to the change law, so as to realize the use of drilling stress measurement instead of drilling cuttings as the main monitoring and early warning index. However, the amount of drilling cuttings and drilling stress are comprehensive indicators including mining stress, mineral properties, and outburst environment, and the mineral seam properties, burial depth, and roof composition of each mineral mine are very different. It is very difficult to find out the relationship between the amount of drilling cuttings and drilling stress by theoretical analysis and calculation. Therefore, by means of case study, the relationship between drilling depth and drilling cuttings and the relationship between bearing pressure distribution and drilling surrounding rock stress in Jisan coal mine are studied, and then the

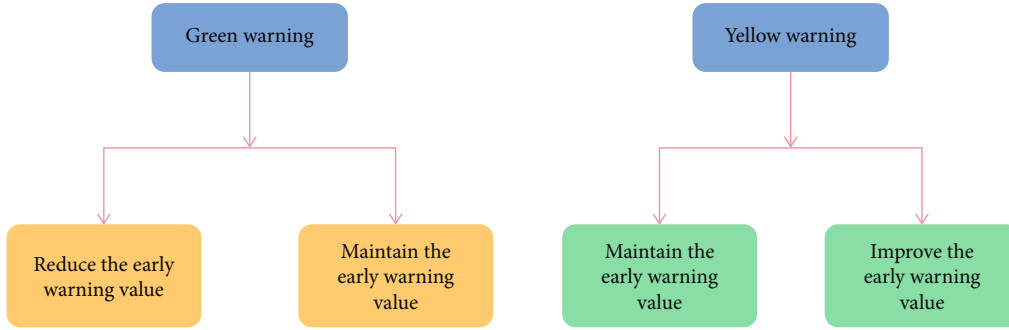


FIGURE 2: Flow chart of early warning value determination method.

TABLE 1: Classification of rock burst according to initial throwing speed.

Rock burst grade	Initial throwing speed
Weak rock burst	$\leq 2$ m/s
Medium rock burst	2-5 m/s
Strong rock burst	5-10
Severe rock burst	$\geq 10$

relationship between drilling cuttings and drilling stress is obtained [20–22].

According to the basic principle of the system and considering the simplicity of field application, the system adopts the method of “single point early warning+process judgment” to predict and early warning the risk of rock burst. Single point early warning refers to the early warning method that sends early warning prompt when the stress value of the stress monitoring point in the monitoring area reaches the set early warning value. Process judgment refers to analyzing the causes of early warning and the law of roof movement on the basis of single point early warning and using the relevant theories of metal mine pressure, so as to further determine the risk degree of the dangerous area and take corresponding measures. The buried depth of borehole stress gauge at a measuring point in the test working face is 8 m. Therefore, it is necessary to calculate the yellow and red zone early warning indicators of borehole surrounding rock stress and drilling cuttings at the depth of 8 m. The key prediction thresholds at the borehole depth of 8 m are:

- (1) Point A: stress value 37 MPa, stress ratio 1.85, with impact risk
- (2) Point B: stress value 26.6 MPa, stress ratio 1.33, no impact hazard
- (3) Point C: the amount of drilling cuttings is 2.8 L/m, which is less than the yellow warning value of 5 L/m, and there is no impact risk
- (4) Point D: the amount of drilling cuttings is 5.2 L/m, which is greater than the yellow warning value of 5 L/M and less than the red warning value of 6.2 L/m. There is a risk of impact, and the yellow warning

- (5) Point E: the amount of drilling cuttings is 6.5 L/m, which is greater than the red prediction value of 6.2 L/m. There is a risk of impact. The red prediction stops production immediately and deals with the dangerous area

The initial setting force of borehole stress gauge with installation depth of 8 m is 6 MPa. The comparison between the monitored relative stress value and the amount of drilling cuttings shows that when the measured stress value reaches 8 MPa, the amount of drilling cuttings reaches 5 L/m; When the measured stress reaches 10 MPa, the amount of drilling cuttings reaches 6.2 L/m. Therefore, the early warning values using the relative stress value as the index are yellow early warning 8 MPa and red early warning 10 MPa. Other boreholes with different depths can use this method to obtain early warning thresholds at different depths. It should be pointed out that the results obtained by the above method are only empirical values, which also need to be tested and corrected by the drilling cuttings method in the mining process of the working face. The specific method is shown in Figure 2.

*3.2. Rock Burst Criterion and Tendency Evaluation Analysis of a Metal Mine.* This is a sudden brittle failure of a certain volume of hard rock accompanied by a certain amount of energy. It is an extremely complex dynamic disaster phenomenon. Rock burst failure can be divided into the following three stages: splitting into plates, shearing into blocks, and ejecting one by one. The cross section of rock burst chamber can be divided into ejection zone and loosening zone, and the loosening zone can be divided into splitting shear zone and splitting zone [23].

The vibration and ejection characteristics of rock burst are the dynamic characteristics that distinguish it from other forms of ground pressure disasters. Vibration characteristics: the vibration caused by rock burst with low intensity is generally weak. Rock burst with high intensity will cause severe vibration effect and release a lot of energy at the same time. Such vibration will even induce secondary damage: the impacted bottom plate will collapse or affect the stability of surface buildings and structures. Ejection characteristics: when rock burst occurs, the pieces of the ejection belt have a certain initial velocity when thrown. The classification of

TABLE 2: Three axis pressure test results of rock samples.

	Lateral stress (MPa)	Failure stress	Elastic modulus (GPa)	Uniaxial compression	Uniaxial tension
$D_3t^a$	10	25.5	61.3	51.1	
	20	220	57.8	98.1	8.52
	30	231	80.8	88.2	
$D_2d^b$	10	125	51.2		
	20	215	54.4	51.1	7.85
	30	257	71.6		
$Sh_{214a}$	10	177	92.6		
	20	180	70.7	98.1	7.21
	30	236	71.6		

rock burst level according to the initial throwing speed is shown in Table 1.

### 3.3. Evaluation of Rock Burst Tendency of Deep Metal Mine.

As one of the few proven hard rock polymetallic mines with a buried depth of up to one kilometer and a mining depth of more than 900 meters, the surrounding rock of the metal mine is limestone, and the proctor's coefficient  $f$  of ore rock is greater than 8, which is moderately stable. Therefore, from the mining depth and the hardness of surrounding rock and ore rock, it shows that the metal mine has a greater possibility of rock burst. The rock samples studied in this paper are taken from the horizontal core of the deep-550 middle section of the mine:  $D_3t^a$  (limestone),  $D_2d^b$  (limestone), and  $Sh_{214a}$  (lead-zinc ore). Uniaxial compressive (tensile) strength and loading and unloading test before peak strength and measurement test of total stress-strain curve were carried out on four core samples [24, 25].

According to the mechanical properties of ore and rock, the triaxial pressure test was carried out in the laboratory of the group company affiliated to the metal mine. The results are shown in Table 2.

**3.3.1. Critical Depth Criterion.** The critical depth criterion of rock burst in different ores and rocks holds that although rock burst mostly occurs in the area with large horizontal tectonic stress, if the burial depth of ketone chamber is large enough, even if it is not affected by tectonic stress and is only affected by the self-weight stress of overlying strata, rock burst may also occur in stone chamber. It considers the effect of self-weight stress and deduces the calculation formula of the minimum buried depth of rock burst caused by different rocks according to the principle of elasticity, that is, the critical depth, as shown in

$$H_{cr} = \frac{0.318R_b(1-\mu)}{(3-4\mu)\gamma}, \quad (1)$$

where  $\mu$  is the Poisson's ratio of rock and  $\gamma$  is the rock gravity (unit:  $N/m^3$ ).

The critical depth of rock burst can be calculated by substituting the rock physical and mechanical parameters

such as uniaxial compressive strength and Poisson's ratio of different rocks into the above formula. See Table 3.

It can be seen from Table 3 that the ore and rock in the middle section of the deep part of the mine -550 m (the surface elevation is -102 m, and the buried depth drop should be 652 m) have reached the critical depth caused by rock burst. The maximum horizontal stress of the metal mine is greater than the vertical stress, and the ratio of horizontal in situ stress to vertical in situ stress is 1.7:1.1. The in situ stress is mainly horizontal tectonic stress [26]. Under this stress distribution, the phenomenon of stress concentration in roadway or stope surrounding rock is more obvious, and the possibility of rock burst in deep stope is greater.

**3.3.2. Elastic Strain Energy Storage Index Method.** Elastic strain energy storage index method refers to the ratio of rock elastic strain energy to consumed strain energy under uniaxial (compression) loading and unloading. That is, the rock burst tendency of rock is determined according to the ability of rock to store elastic strain energy. The expression of this method is shown in

$$K_u = \frac{u}{u_1}, \quad (2)$$

where  $u$  is the retained elastic strain energy and  $u_1$  is the strain energy loss.

The judgment basis of this method is shown in

$$\begin{aligned} K_u &< 2.0, \\ 2.0 &< K_u < 5.0, \\ 5.0 &< K_u. \end{aligned} \quad (3)$$

According to the retained elastic strain energy  $u$  and loss strain energy  $u_1$  measured in the experiment, the elastic strain energy index  $K_u$  is calculated. The calculation results are shown in Table 4.

**3.3.3. Strength Brittleness Coefficient Method.** The rock burst tendency of rock is determined by the ratio of uniaxial compressive strength  $R_c$  to tensile strength  $R_t$ . The expression is shown in

$$R = \frac{R_c}{R_t}. \quad (4)$$

According to the general law, the greater the rock  $R$ , the stronger the brittleness, that is, the greater the possibility of rock burst. The criterion of this method is shown in

$$\begin{aligned} R &< 10, \\ 10 &< R \leq 18, \\ 18 &< R. \end{aligned} \quad (5)$$

According to the uniaxial compressive strength  $R_c$  and tensile strength  $R_t$  measured in the experiment, the strength

TABLE 3: Critical depth of rock burst of surrounding rock and ore body in the middle section of -550 m.

Lithology	Uniaxial compressive strength (MPa)	Poisson's ratio	Unit weight (kN/m <sup>3</sup> )	Critical depth (m)
$D_3t^a$	88.2	0.21	13.6	505
$D_2d^b$	51.1	0.35	25.7	511
$Sh_{214}^a$	98.1	0.32	12.4	470

TABLE 4: Evaluation of rock burst tendency based on strength strain energy index.

	$D_3t^a$	$D_2d^b$	$Sh_{214}^a$
$u$	12	463.1	566.0
$u_1$	5	128.0	52.0
$K_u$	2.12	3.30	10.8
Rock burst propensity	Medium	Medium	Strong

TABLE 5: Evaluation of rock burst tendency based on strength brittleness coefficient.

	$D_3t^a$	$D_2d^b$	$Sh_{214}^a$
$R_c$	62.71	84.24	103.85
$R_t$	4.81	5.04	5.1
R	11.86	15.8	15.82
Rock burst propensity	Medium	Medium	Medium

brittleness coefficient  $R$  is calculated. The calculation results are shown in Table 5.

**3.3.4. Deformation Brittleness Coefficient Method.** According to the stress-strain curve before the peak load of rock, the total deformation ( $U$ ) and permanent deformation ( $UL$ ) before the peak load of rock are obtained by loading and unloading to judge and evaluate the rock burst tendency of the rock. The method expression is shown in

$$k_u = \frac{u}{ul}. \quad (6)$$

Generally speaking, the greater the  $k_u$ , the greater the brittleness of the rock and the greater the tendency of rock burst. The discrimination index is shown in

$$\begin{aligned} K_u &< 2.0, \\ 2.0 &\leq K_u \leq 6.0, \\ 6.0 &\leq K_u \leq 9.0, \\ 9.0 &\leq K_u. \end{aligned} \quad (7)$$

This judgment method needs to determine the total deformation and permanent deformation before the peak

value of ore and rock, calculate its brittleness coefficient according to the expression, and finally judge the rock burst tendency of ore and rock according to the criterion. Choose to load to about 90% of the peak strength of rock and start unloading stress. The evaluation of rock burst tendency after relevant ore and rock experiments is shown in Table 6.

It can be seen from the calculation results that all rocks of the core samples taken in the deep have medium rock burst tendency. Although all the calculation results and their tendency evaluation are not completely consistent, this is caused by the different influence weights of various indicators and the discreteness of the experimental data. Nevertheless, the surrounding rock and ore body in the middle section of -550 m of the metal mine still have different degrees of rock burst tendency.

**3.4. Research on Rock Burst Early Warning Model Based on Microseismic Monitoring Technology.** The purpose of introducing microseismic monitoring system is to monitor the change of ground pressure activity caused by mining in real time, grasp the change law of various parameters and indexes before the occurrence of ground pressure disaster, and finally put forward a disaster early warning model suitable for different situations of each mine according to the theoretical and actual monitoring situation and the current situation of on-site mining.

**3.4.1. Relationship between Magnitude and Frequency of Microseismic Events.** Through the summary of multiple rock burst data, the microseismic events induced by mining follow the same rules as natural earthquakes. By analyzing the activity characteristics of the two types of earthquakes, it is found that they all follow the frequency magnitude relationship described by Gutenberg Richter. This relationship applies to any magnitude range. That is, by studying the microseismic magnitude frequency distribution within a specified time interval  $[a, b]$ , a group of magnitude random variables  $\{M_i; t \in [a, b]\}$  can be obtained. For the target monitoring area, the relationship between event frequency and magnitude obeys index, as shown in

$$n(M) = N_0 e^{-bM}. \quad (8)$$

In the above formula,  $n(M)$  is the number of microseismic events with magnitudes from  $M$  to  $M + DM$  in a certain period in the target area, i.e., differential frequency. It can also be expressed by the cumulative frequency of microseismic events.

The total number (cumulative frequency) of events with magnitude greater than  $m$  in a period of time is shown in

$$N(M) = \int n(M) dM. \quad (9)$$

Similarly, as shown in

$$\lg N(M) = A - bM, \quad (10)$$

where  $A = a - \lg(b \ln 10)$ , the two unknowns  $a$  and  $b$  are

TABLE 6: Evaluation of rock burst tendency based on deformation brittleness coefficient.

	$D_3 t^a$	$D_2 d^b$	$Sh_{214} a$
$u$	0.0136	0.0102	0.0128
$ul$	0.001	0.0014	0.00116
$kl$	6.24	5.76	10.01
Rock burst propensity	Medium	Medium	Strong

constant in the determined target monitoring area.  $a$  describes the overall level of ground pressure activity in the target area, which is related to the total number of event samples above earthquake magnitude  $M$ , indicating the microseismic activity degree, which is called microseismic activity parameter.  $b$  is a parameter describing the magnitude distribution, which is generally close to 1, representing the relative number of small magnitude events and large magnitude events in the target monitoring area in a specific time period. Together with  $a$ , it is called microseismic activity parameter, which indicates the degree of ground pressure activity in different senses. Figure 3 shows the magnitude frequency relationship of microseismic events in the target monitoring area over a period of time.

$B$  value represents the proportional relationship between the number of large and small magnitude events. It represents the process state of rock mass medium failure development in the target monitoring area, but the premise is that all microseismic events above a lower limit magnitude ( $m$ ) can be monitored within a period of time by calculating the value of  $B$  in the area.

In a constant short time, the relationship between the maximum amplitude of microseismic event per unit amplitude and crack volume satisfies the following formula, as shown in

$$A \in V_V^{2/3}, \quad (11)$$

where  $V_V$  corresponds to the fracture volume of a microseismic event, that is, the damage failure volume.

Only one event is generated and its diameter is  $r$ , and its amplitude is shown in

$$A \in r^2. \quad (12)$$

The number of events  $n$  is shown in

$$N \in r^{-2b}. \quad (13)$$

According to the definition of capacity dimension, the dimension formula (14) is obtained:

$$D_f = \lim_{r \rightarrow 0} \frac{\ln N(r)}{\ln (1/r)} = 2b. \quad (14)$$

It is obvious from the formula that the capacity dimen-

sion  $D_f$  is the same as the microseismic activity parameter  $B$ , and the value is twice the value of  $B$ .

Many observations and studies show that the capacity dimension of rock mass decreases before failure. In the quiet period and the increase of capacity dimension, the probability of rock burst is low, and the smaller  $D_f$  is, the greater the magnitude of microseismic event is.

The increase of  $D_f$  indicates that the roughness of rock mass cracks is increasing. During this period, the rock mass is in the stage of crack compaction and propagation. The proportion of small magnitude events in the total events is greater than that of large magnitude events, that is, the increase of  $D_f$  does not necessarily cause rock burst damage. The probability of agreed occurrence is 0~25%.

The decrease of  $D_f$  indicates that the roughness of rock mass cracks is reduced and the failure speed of rock mass is accelerated. The number of large magnitude events in the total events is greater than that of small magnitude events. In other words, the reduction of  $D_f$  will lead to a greater probability of rock burst disaster. The probability of occurrence of the agreement is 50%.

$D_f$  is in a quiet period, the crack development of rock mass is relatively stable, and generally, it will not be damaged. The probability of occurrence of the agreement is 25%.

When the rock mass is damaged, the  $D_f$  value first decreases and then increases or is relatively calm. The smaller the descending area is, the greater the damage capacity of rock burst disaster may be.

#### 3.4.2. Adjoint Relationship between Energy Index and Cumulative Apparent Volume.

The process of crack propagation and evolution in rock mass is the basis of rock burst or other large-scale damage. The internal defects or weak areas of rock mass are gradually activated and intensified under the continuous influence of mining. This process will trigger microseismic events with different magnitudes and energies. When a certain capacity threshold is reached, microseismic sensors installed nearby will be triggered. Therefore, the microseismic system can record the fracture propagation process in the form of wave and quantify the fracture evolution process by the information contained in the recorded stress wave.

The average energy can be obtained from the relationship between the measured average capacity and microseismic potential  $P$  in the selected area, as shown in

$$EI = \frac{E}{E(p)} = \frac{E}{10^{d \log P+c}}. \quad (15)$$

Apparent volume  $V$  is the source volume that represents the volume of inelastic deformed rock mass generated in the focal area when microseismic events occur, as shown in

$$V = \frac{P}{\varepsilon_A} = \frac{\mu p^2}{E}. \quad (16)$$

In the formula,  $E$  is the rock shear modulus, namely

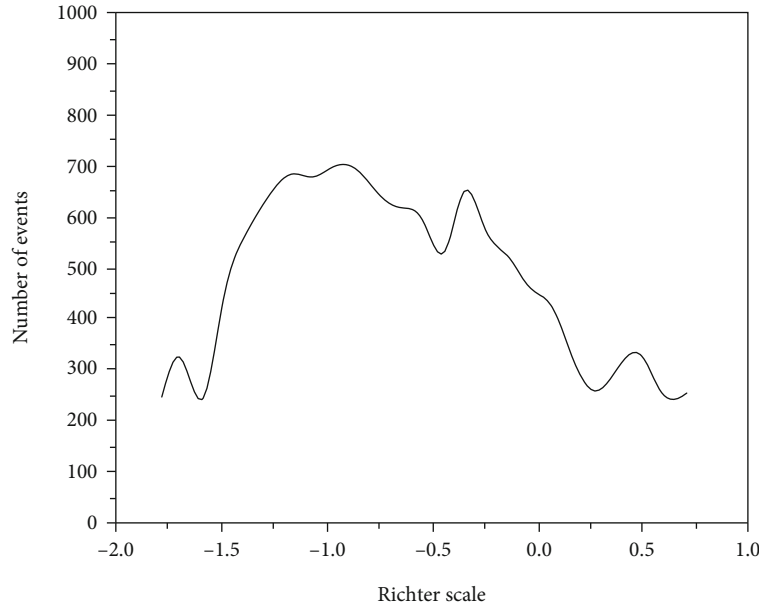


FIGURE 3: Magnitude frequency relationship of microseismic events in the target monitoring area over a period of time.

TABLE 7: Early warning value of real-time monitoring and early warning system of rock burst in 3305 working face.

Measuring point depth/ m	Early warning level	Early warning value
8	Green display	<10
	Yellow warning	10~12
	Red warning	>12
14	Green display	<13
	Yellow warning	13~15
	Red warning	>15

stiffness. The apparent volume  $V$  as a scalar can be easily expressed in terms of cumulants.

The larger the microseismic energy index in a region, the greater the focal driving stress at the time of the event. The cumulative apparent volume with the increase of energy index indicates the strain hardening process. The apparent volume with the decrease of energy index and the development of acceleration represents the strain softening process, which indicates that the rock mass enters an unstable state.

Metal mine activity has rheological properties. There are four independent parameters in quantitative seismology to describe this rheological properties, namely, seismic apparent stress, seismic stiffness, seismic strain rate, and seismic diffusivity, while the Schmidt number is the ratio of earthquake radiance to earthquake diffusivity.

## 4. Result Discussion

### 4.1. Application of Early Warning System Based on Deep Learning Data Analysis in the First Mining Face of Kilometer Metal Mine

4.1.1. *Project Overview.* During the excavation of 3305 face in a mine, dynamic phenomena such as some bolt pulling

off have occurred many times, which has brought influence and potential threat to safety production. In order to ensure the safe mining of this working face, a real-time monitoring and early warning system of rock burst is installed before mining. Ten groups of measuring points are arranged in the upper and lower grooves of the working face, with a spacing of 25 m. Two borehole stress meters are arranged in each group of measuring points, and the buried depths are 8 and 14 m, respectively. According to the above early warning value setting method, through the analysis of ground pressure observation and drilling cuttings method monitoring data at the initial stage of mining, the preliminarily set early warning values are shown in Table 7.

4.1.2. *Early Warning Process Analysis.* On the first day, the cumulative footage of the working face is 35 m, and the second group of measuring points with a depth of 8 m on the track (50 m from the cutting hole and 15 m from the working face) sends a yellow warning. At this time, the cumulative footage of the working face is 35 m. On the third day, the cumulative footage of the working face is 39 m, the measuring point is 11 m away from the working face, the stress reaches the peak, and the system sends a red warning, as shown in Figure 4. Immediately, the monitoring personnel informed the underground construction personnel to drill additional large-diameter pressure relief holes on both sides of the measuring point for pressure relief. With the continuous mining of the working face, the mineral in front of the working face is plastic damaged and the stress decreases gradually. After 10 days, the cumulative footage of the working face is 45.5 m, the measuring point is 4.5 m away from the working face, and the stress of the measuring point decreases to the green display value. The stress variation is shown in Figure 5.

Through comprehensive analysis of other ground pressure monitoring data, the reason for this early warning is



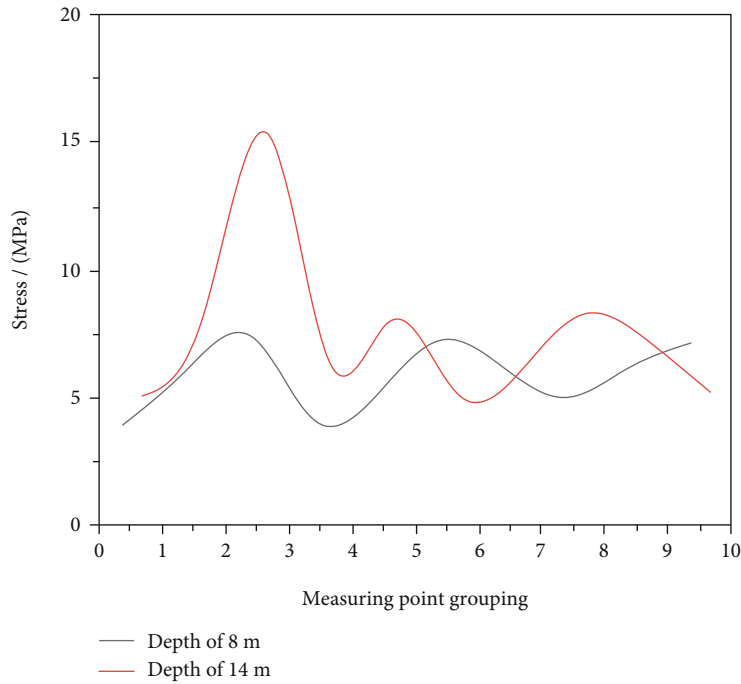


FIGURE 4: Real-time stress histogram of the system.

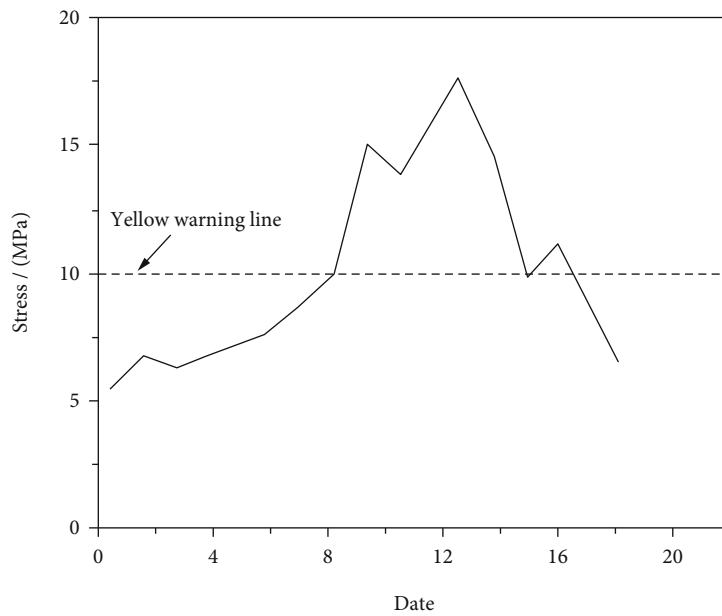


FIGURE 5: Stress change curve of early warning measuring point.

the initial pressure of the working face. According to the measured results, when the working face advances to 35~45 m, it is the initial pressure stage.

*4.1.3. Analysis of Early Warning Process of Fault Risk Area.* When the cumulative footage of the working face is 120 m, the stress of the fourth group of measuring points with a depth of 14 m (at this time, the measuring point is 170 m away from the working face) begins to rise. When the cumulative footage of the working face is 190 m (at this time, the measuring point is 100 m away from the working face), the

stress value of the measuring point reaches the yellow warning value. Then, with the promotion of the working face, the pressure of the measuring point continues to rise, and the maximum stress reaches 22 MPa. The stress change process is shown in Figure 6.

When the cumulative footage of the working face is 350 m (the measuring point is 390 m from the cutting hole and 40 m from the working face), rock blasting occurs, and the stress of the measuring point of the monitoring system suddenly decreases. The early warning measuring point is just in front of the fault. Through analysis, it can be seen that

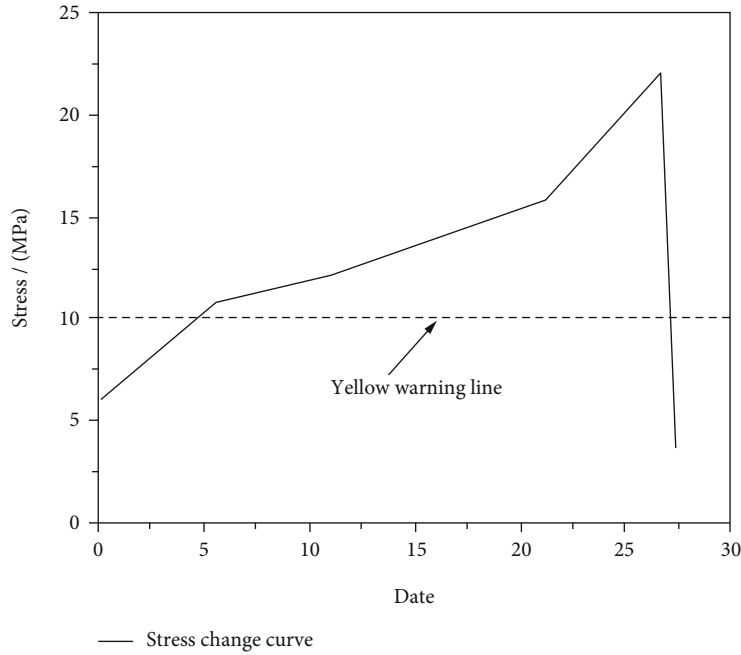


FIGURE 6: Stress variation curve of fault early warning measuring point.

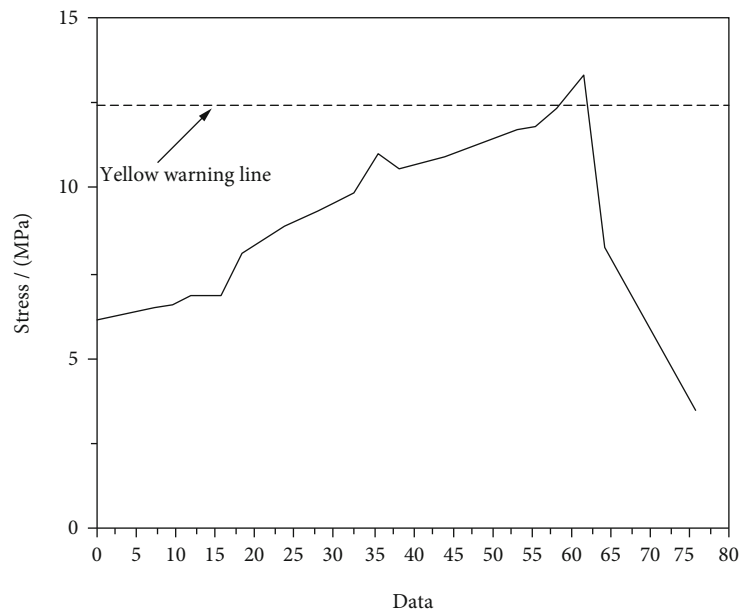


FIGURE 7: Stress recovery curve of measuring point.

the early warning is caused by fault tectonic stress. Because the stress of other measuring points near the early warning measuring point is low, it shows that the influence range of tectonic stress and mining stress generated by the fault is small, and there is little possibility of large impact. According to the measured data of this early warning, when the working face advances to 170 m in front of the fault, it enters the fault influence area. When the working face advances to 100 m in front of the fault, it enters the high stress area formed by the superposition of fault tectonic stress and mining stress. When the working face advances to 40 m in front

of the fault, the stress reaches the maximum, and it is very easy to induce rock burst in this section.

#### 4.2. Application of Early Warning System in Deep Mining Face

4.2.1. Project Overview. The mining depth of 2103 working face in a provincial mine is 900~1100m. since the beginning of excavation, there have been 10 mine earthquakes. At 4:28 a.m. one day, a mine earthquake occurred in this area. The maximum distance of roof and floor was 3.3m, injuring 6

people, including 1 death. Microseismic monitoring shows that it is  $1.28 \times 10^7$  J mine earthquake destroyed nearly 260m of the roadway. A total of 40 measuring points are arranged in the working face system, and 10 groups of measuring points are arranged in the upper and lower grooves, with a spacing of 25m. the embedding depth of borehole stress meters of each group of measuring points is 12.17m.

*4.2.2. Inspection and Early Warning of Pressure Relief Works by Monitoring and Early Warning System.* In order to ensure the safety of the working face, pre pressure relief treatment is carried out before resuming mining. The specific parameters for pressure relief of large-diameter deep holes in the mining wall are borehole diameter 110 mm, borehole depth 25 m, and borehole spacing 3 m. The stress measuring points of the early warning system are arranged in the pressure relief area to monitor the change trend of stress recovery in the pressure relief area. After the production of the working face is resumed, the rock burst is used online.

The monitoring and early warning system starts to monitor the advance stress. With the mining of the working face, the stress increases gradually. When the red warning value is reached, the secondary pressure relief is immediately carried out near the warning measuring point to reduce the stress to the safe range, as shown in Figure 7.

After the production of the working face is resumed, the real-time monitoring and early warning system of rock burst is installed, and the early warning situation is handled in time. Although there are many metal mine earthquakes, due to the pressure relief effect, sufficient protective belts are formed on both sides of the roadway, the control goal of "earthquake without disaster" is realized, and the safe mining of the working face is ensured.

## 5. Conclusion

With the continuous progress of science and technology and the deepening of economic development, the demand for nonferrous metals only increases. Therefore, it is necessary to further improve the utilization rate of mineral resources and overcome the waste phenomenon of mining mass mining caused by limited mining technology. In this paper, ground pressure monitoring and early warning based on in-depth learning data analysis are carried out for the deep ore and rock of a metal mine, and an early warning zoning method combining large zoning and small zoning is proposed. Zoning classification monitoring is realized in monitoring, and the combination of overall early warning in large zoning and local early warning in small zoning is realized in early warning, and the pertinence of rock burst monitoring parameter selection and the field applicability of the platform system are improved. Upgrade and develop based on the original platform system, realize the intelligent linkage and automatic reporting functions such as mine and anticour research center, well and underground, static and dynamic data, early warning results, and on-site disposal measures, improve the timeliness of rock burst monitoring, early warning and management, solve some anticour problems existing in Yankuang Group, and reduce the labor cost.

## Data Availability

No data were used to support this study.

## Conflicts of Interest

The authors declare that there are no conflicts of interest regarding the publication of this article.

## Acknowledgments

This work was supported by the China National Key R&D Program during the 14th Five-year Plan Period (Grant No. 2021YFC2900400).

## References

- [1] A. Boukari, S. Benabdallah, E. Everbecq et al., "Assessment of agriculture pressures impact on the Joumine river water quality using the Pegase model," *Environmental Management*, vol. 64, no. 4, pp. 520–535, 2019.
- [2] G. Lackey and H. Rajaram, "Modeling gas migration, sustained casing pressure, and surface casing vent flow in onshore oil and gas wells," *Water Resources Research*, vol. 55, no. 1, pp. 298–323, 2019.
- [3] Y. Cai, Z. Xie, J. Wang, W. Peng, and X. Geng, "Reply to the discussion by Mesri and Kane on "New approach of vacuum preloading with booster prefabricated vertical drains (PVDs) to improve deep marine clay strata,"" *Canadian Geotechnical Journal*, vol. 56, no. 12, pp. 2017–2017, 2019.
- [4] M. Ambrosiano, M. T. Bevacqua, T. Isernia, and V. Pascazio, "The tomographic approach to ground-penetrating radar for underground exploration and monitoring: a more user-friendly and unconventional method for subsurface investigation," *IEEE Signal Processing Magazine*, vol. 36, no. 4, pp. 62–73, 2019.
- [5] J. Thomas, E. Stonebrook, B. Klammer, H. P. Patel, and M. Kallash, "Challenges of diagnosing pediatric hypertension using ambulatory blood pressure monitoring," *Pediatric Nephrology*, vol. 36, no. 2, pp. 373–378, 2021.
- [6] C. A. Tschan, V. Sanchez, M. Heckelmann, and S. Antes, "Home telemonitoring of intracranial pressure," *Acta Neurochirurgica*, vol. 161, no. 8, pp. 1605–1617, 2019.
- [7] S. T. Robinson, J. P. Villagrasa, M. McGarrigle, G. P. Duffy, and A. C. Cameron, "Pc190. A pressure-sensing clip for measuring and monitoring sub-bandage pressure during treatment of venous leg ulcers," *Journal of Vascular Surgery*, vol. 69, no. 6, pp. e256–e257, 2019.
- [8] S. Worthington and A. E. Foley, "Deriving celerity from monitoring data in carbonate aquifers," *Journal of Hydrology*, vol. 598, no. 3, article 126451, 2021.
- [9] T. Kanabkaew, P. Mekbungwan, S. Raksakietisak, and K. Kanchanasut, "Detection of PM<sub>2.5</sub> plume movement from IoT ground level monitoring data," *Environmental Pollution*, vol. 252, no. 1, pp. 543–552, 2019.
- [10] C. D. Río, F. Lobos, A. Siegmund, C. Tejos, and J. L. García, "Gofos, ground optical fog observation system for monitoring the vertical stratocumulus-fog cloud distribution in the coast of the Atacama desert, Chile," *Journal of Hydrology*, vol. 597, no. 3–4, article 126190, 2021.
- [11] E. V. Romashchenko, I. O. Girka, and A. A. Bizyukov, "Effect of background gas pressure on macroparticles in cathodic arc

- plasma deposition,” *IEEE Transactions on Plasma Science*, vol. 47, no. 3, pp. 1494–1499, 2019.
- [12] L. C. Chen, “A plug-and-play high-pressure ESI source with an emitter at ground potential and its application to high-temperature capillary LC-MS,” *Journal of the American Society for Mass Spectrometry*, vol. 31, no. 5, pp. 1015–1018, 2020.
- [13] H. Ma, Y. Long, M. Zhong, X. Li, and X. Xie, “Study on ground vibration mode of physical explosion of high pressure natural gas pipeline,” *Acoustical Physics*, vol. 65, no. 5, pp. 583–592, 2019.
- [14] M. Oz, C. Kaya, E. Olmezogullari, and M. S. Aktas, “On the use of generative deep learning approaches for generating hidden test scripts,” *International Journal of Software Engineering and Knowledge Engineering*, vol. 31, no. 10, pp. 1447–1468, 2021.
- [15] S. Sengupta, A. Singh, H. A. Leopold, T. Gulati, and V. Lakshminarayanan, “Ophthalmic diagnosis using deep learning with fundus images - a critical review,” *Artificial Intelligence in Medicine*, vol. 102, p. 101758, 2020.
- [16] P. R. Srivastava, Zuopeng (Justin) Zhang, and P. Eachempati, “Deep neural network and time series approach for finance systems,” *Journal of Organizational and End User Computing (JOEUC)*, vol. 33, no. 5, pp. 204–226, 2021.
- [17] Y. Li, Y. Zuo, H. Song, and Z. Lv, “Deep learning in security of Internet of Things,” *IEEE Internet of Things Journal*, vol. PP (99), pp. 1–1, 2021.
- [18] G. Xiao, Q. Cheng, and C. Zhang, “Detecting travel modes using rule-based classification system and Gaussian process classifier,” *IEEE Access*, vol. 7, pp. 116741–116752, 2019.
- [19] Y. Liu and F. Guifang, “Emotion recognition by deeply learned multi-channel textual and EEG features,” *Future Generation Computer Systems*, vol. 119, pp. 1–6, 2021.
- [20] M. A. Rahman, M. S. Hossain, N. A. Alrajeh, and N. Guizani, “B5g and explainable deep learning assisted healthcare vertical at the edge: covid-19 perspective,” *IEEE Network*, vol. 34, no. 4, pp. 98–105, 2020.
- [21] S. Li and Y. Yang, “Hierarchical deep learning for data-driven identification of reduced-order models of nonlinear dynamical systems,” *Nonlinear Dynamics*, vol. 105, no. 4, pp. 3409–3422, 2021.
- [22] H. Gu, Y. P. Xu, D. Ma, J. Xie, and Z. Bai, “A surrogate model for the variable infiltration capacity model using deep learning artificial neural network,” *Journal of Hydrology*, vol. 588, no. 12, article 125019, 2020.
- [23] K. Song, M. Wang, L. Liu, C. Wang, and B. Yang, “Intelligent recognition of milling cutter wear state with cutting parameter independence based on deep learning of spindle current clutter signal,” *International Journal of Advanced Manufacturing Technology*, vol. 109, no. 3-4, pp. 929–942, 2020.
- [24] B. Karg and S. Lucia, “Efficient representation and approximation of model predictive control laws via deep learning,” *IEEE Transactions on Cybernetics*, vol. 50, no. 9, pp. 3866–3878, 2020.
- [25] F. Huang, J. Zhang, C. Zhou, Y. Wang, and L. Zhu, “A deep learning algorithm using a fully connected sparse autoencoder neural network for landslide susceptibility prediction,” *Landslides*, vol. 17, no. 1, pp. 217–229, 2020.
- [26] M. K. Goenka, U. Goenka, S. Afzalpurkar, S. C. Tiwari, and I. K. Tiwary, “Role of static and dynamic intra-abdominal pressure monitoring in acute pancreatitis: a prospective study on its impact,” *Pancreas*, vol. 49, no. 5, pp. 663–667, 2020.